

Towards the IR Detection of Carbonic Acid: Absorption and Emission Spectra

Ryan C. Fortenberry

r410@olemiss.edu

Department of Chemistry & Biochemistry, University of Mississippi, University, Mississippi
38677-1848, U.S.A.

Vincent J. Esposito

NASA Ames Research Center, MS N245-3, Moffett Field, California 94035, U.S.A.

January 25, 2024

Received _____; accepted _____

ABSTRACT

With the recent radioastronomical detection of *cis-trans*-carbonic acid (H_2CO_3) in a molecular cloud toward the galactic center, the more stable but currently unobserved *cis-cis* conformer is shown here to have strong IR features. While the higher-energy *cis-trans*-carbonic acid was detected at millimeter and centimeter wavelengths, owing to its larger dipole moment, the vibrational structure of *cis-cis*-carbonic acid is more amenable to its observation at micron wavelengths. Even so, both conformers have relatively large IR intensities, and some of these fall in regions not dominated by polycyclic aromatic hydrocarbons. Water features may inhibit observation near the $2.75\ \mu\text{m}$ hydride stretches, but other vibrational fundamentals and even overtones in the $5.5\ \mu\text{m}$ to $6.0\ \mu\text{m}$ range may be discernible with JWST data. This work has employed high-level, accurately benchmarked quantum chemical anharmonic procedures to compute exceptionally accurate rotational spectroscopic data compared to experiment. Such performance implies that the IR absorption and even cascade emission spectral features computed in this work should be accurate and will provide the needed reference for observation of either carbonic acid conformer in various astronomical environments.

1. Introduction

The recent detection (Sanz-Novo et al. 2023) of carbonic acid (H_2CO_3) towards the galactic center in molecular cloud G+0.693-0.027 via the Yebes 40 m and IRAM 30 m telescopes is the culmination of more than 25 years of speculation about the presence of this molecule in the interstellar medium (ISM) beyond its role in solar system ices (Strazzulla et al. 1996; Zheng & Kaiser 2007; Peeters et al. 2010; Jones et al. 2014; Sandford et al.

2020).

Carbonic acid is well-known to be significantly less stable than its related formic and other carboxylic acid molecular family members even though it is comprised of a ketone and two hydroxyl groups. The reason is that H_2CO_3 readily dissociates into water and carbon dioxide with a barrier of roughly 40 kcal/mol and thermodynamically lies about 10 kcal/mol above the H_2O and CO_2 products (Kumar et al. 2007). However, this implies that it should form relatively easily from moderately-processed ices comprised of these abundant and volatile molecules (Jones et al. 2014; Wang & Bürgi 2021). Surface association of the *cis*- or *trans*-HOCO radical with the hydroxyl radical is the most likely formation pathway for carbonic acid (Sanz-Novo et al. 2023; Noble et al. 2011; Ioppolo et al. 2021), but other mechanisms are not outside of the realm of possibility. Regardless of the exact chemical mechanism, as most astrophysical ices are largely comprised of water mixed with some form of carbon oxide material (i.e. methanol, formaldehyde, carbon monoxide, carbon dioxide, etc.), carbonic acid is almost certainly created in such ices. Even though the vaporization of carbonic acid into the gas-phase could, again, quickly break this ketone-diol down into water and carbon dioxide as part of this process, some should survive long enough in the gas-phase to be observed. This recent detection is strong evidence to support the idea that it will persist in the gas-phase.

The conclusive observation of gas-phase, astronomical carbonic acid still provides novel twists to the story of this seemingly simple but often complicated molecule. The most stable form of H_2CO_3 is actually the observed *cis-cis* conformer at roughly 2 kcal/mol lower in energy than the *cis-trans* arrangement (Wallace & Fortenberry 2021), but the dipole moment of *cis-cis* is 0.2 D. The *cis-trans* form, on the other hand, has a dipole moment of more than 3.0 D (Mori et al. 2011; Sanz-Novo et al. 2023). Hence, the higher-energy conformer has been observed. The *trans-trans* conformer is a transition state between equivalent

cis-trans conformers. The relatively low-energy separation between the two minimum energy structures implies that both will be present in most astronomical environments like the ISM. It follows then that if the higher-energy *cis-trans* is observed, the *cis-cis* conformer will almost certainly be present, as well. However, the small dipole moment implies that radioastronomical tools cannot be utilized for its ready detection, but an upper-limit has been established (Sanz-Novo et al. 2023). However, the advent of the *James Webb Space Telescope* (JWST) provides another avenue for potential observation of the lower energy conformer.

While the rotational spectrum of *cis-cis*-H₂CO₃ has been known for more than a decade (Mori et al. 2011), the IR spectrum of either conformer is less-well established. Computational (Huber et al. 2012; Reddy et al. 2012; Sagiv et al. 2018) and Ne/Ar-matrix experimental (Bernard et al. 2011) studies have provided insights into the vibrational features of carbonic acid, but gas-phase experimental or high-level quantum chemical classification of the IR characteristics of any conformer are currently lacking from the literature. As a result, the best chance to observe *cis-cis*-carbonic acid will come from comparison of JWST observations to newly reported spectral data. The present work will compute exceptionally high-accuracy quantum chemical characterization of both conformers of carbonic acid in order to provide the means for the first astronomical observation of *cis-cis*-H₂CO₃ as well as IR observation of the known *cis-trans*. Locating astronomical environments where both conformers of carbonic acid reside as determined from remote observations requiring comparison to accurate standards will also assist in analysis of how UV photons affect its potential role in electronic spectral properties in ices and disks (Ioppolo et al. 2021; Wallace & Fortenberry 2021, 2022; Haney et al. 2023).

One of the most accurate quantum chemical approaches for producing rovibrational spectral data utilizes coupled cluster theory at the singles, doubles, and perturbative triples

method with the explicitly correlated formalism, CCSD(T)-F12b, (Raghavachari et al. 1989; Shavitt & Bartlett 2009; Crawford & Schaefer III 2000; Adler et al. 2007; Knizia et al. 2009) along with the core-correlating cc-pCVTZ-F12 basis set (Dunning 1989; Peterson & Dunning 2002; Yousaf & Peterson 2008; Peterson et al. 2008; Hill & Peterson 2010). The triple- ζ basis set is sufficient for large basis set approximations due to explicit correlation accelerating convergence to the complete basis set limit (Györffy & Werner 2018). These energies are then corrected for canonical CCSD(T) scalar relativity (Douglas & Kroll 1974). These electronic energies are conjoined to a quartic force field (QFF), a fourth-order Taylor series expansion of the potential portion of the internuclear Watson Hamiltonian (Fortenberry & Lee 2019, 2022). This so-called F12-TcCR (for explicitly correlated, triple- ζ , core correlating, relativistic) QFF has been shown to provide exceptional accuracy for comparison to known experimental standards often to within 1 cm^{-1} or better for organic molecules including the related methanediol where this method confirmed its gas-phase synthesis (Westbrook & Fortenberry 2020; Watrous et al. 2021; Zhu et al. 2011; Jian et al. 2021; Davis et al. 2022). Furthermore, IR emission can also now be computed to high accuracy and done so in full cascade (Mackie et al. 2018a) in order to provide a clear comparison to JWST observations. Both methods will be employed in this work in order to give the clearest characterization yet as to the IR observation of carbonic acid in both its lower-energy *cis-cis* and its radioastronomically-observed *cis-trans* conformers.

2. Computational Details

2.1. F12-TcCR QFF

The F12-TcCR QFF procedure (Watrous et al. 2021) begins with a tight, core correlating CCSD(T)-F12b/cc-pCVTZ-F12 geometry optimization of the molecular structure. The geometry is then displaced by 0.005 \AA and 0.005 radians per the following

symmetry-internal coordinate system for C_{2v} *cis-cis*-H₂CO₃:

$$S_1(a_1) = O_1 = C \quad (1)$$

$$S_2(a_1) = \frac{1}{\sqrt{2}}[(C - O_2) + (C - O_3)] \quad (2)$$

$$S_3(a_1) = \frac{1}{\sqrt{2}}[(O_2 - H_1) + (O_3 - H_2)] \quad (3)$$

$$S_4(a_1) = \frac{1}{\sqrt{2}}[\angle(O_1 - C - O_2) + \angle(O_1 - C - O_3)] \quad (4)$$

$$S_5(a_1) = \frac{1}{\sqrt{2}}[\angle(C - O_2 - H_1) + \angle(C - O_3 - H_2)] \quad (5)$$

$$S_6(b_2) = \frac{1}{\sqrt{2}}[(C - O_2) - (C - O_3)] \quad (6)$$

$$S_7(b_2) = \frac{1}{\sqrt{2}}[(O_2 - H_1) - (O_3 - H_2)] \quad (7)$$

$$S_8(b_2) = \frac{1}{\sqrt{2}}[\angle(O_1 - C - O_2) - \angle(O_1 - C - O_3)] \quad (8)$$

$$S_9(b_2) = \frac{1}{\sqrt{2}}[\angle(C - O_2 - H_1) - \angle(C - O_3 - H_2)] \quad (9)$$

$$S_{10}(b_1) = OPB(O_1 - C - O_2 - O_2) \quad (10)$$

$$S_{11}(b_1) = \frac{1}{\sqrt{2}}[\tau(O_1 - C - O_2 - H_1) - \tau(O_1 - C - O_3 - H_2)] \quad (11)$$

$$S_{12}(a_2) = \frac{1}{\sqrt{2}}[\tau(O_1 - C - O_2 - H_1) + \tau(O_1 - C - O_3 - H_2)], \quad (12)$$

where OPB stands for “out-of-plane-bend” and O₁ is understood to be the ketone oxygen. This produces 4493 total points. For C_s *cis-trans*-H₂CO₃ there are 8965 total

points constructed from the following simple-internal coordinate system:

$$S_1(a') = O_1 = C \quad (13)$$

$$S_2(a') = C - O_2 \quad (14)$$

$$S_3(a') = C - O_3 \quad (15)$$

$$S_4(a') = O_2 - H_1 \quad (16)$$

$$S_5(a') = O_3 - H_2 \quad (17)$$

$$S_6(a') = \angle(O_1 - C - O_2) \quad (18)$$

$$S_7(a') = \angle(O_1 - C - O_3) \quad (19)$$

$$S_8(a') = \angle(C - O_2 - H_1) \quad (20)$$

$$S_9(a') = \angle(C - O_3 - H_2) \quad (21)$$

$$S_{10}(a'') = OPB(O_1 - C - O_2 - O_2) \quad (22)$$

$$S_{11}(a'') = \tau(O_1 - C - O_2 - H_1) \quad (23)$$

$$S_{12}(a'') = \tau(O_1 - C - O_3 - H_2) \quad (24)$$

with the understanding that H_2 is the hydrogen atom creating the *trans* conformer.

At each point F12-TcCR energies are computed via MOLPRO2020.1 (Werner et al. 2012, 2022). These are then fit via a least-squares procedure, transformed into Cartesian coordinates, and treated with rotational and vibrational perturbation theory at second-order, VPT2, (Mills 1972; Watson 1977; Papousek & Aliev 1982) as available in the PBQFF program (Westbrook & Fortenberry 2023) built upon the SPECTRO program (Gaw et al. 1991). Fermi resonance polyads can be treated within VPT2 in this program (Martin et al. 1998) for increased accuracy and are detected automatically with refinements made by the user. For *cis-cis*-carbonic acid, these include: $2\nu_3=\nu_1$; $2\nu_7=\nu_9+\nu_6=\nu_{11}+\nu_5=\nu_3$; $\nu_9+\nu_7=\nu_{12}+\nu_8=\nu_4$; $2\nu_{10}=\nu_{10}+\nu_8=\nu_5$; $\nu_{12}+\nu_8=\nu_{12}+\nu_{10}=\nu_6$; & $2\nu_{11}=2\nu_{12}=\nu_7$. For *cis-trans*-carbonic acid, the Fermi resonance polyads are comprised

of: $2\nu_7=\nu_9+\nu_4=\nu_9+\nu_5=\nu_{11}+\nu_4=\nu_{11}+\nu_6=\nu_3$; $2\nu_8=\nu_9+\nu_7=\nu_{10}+\nu_8=\nu_{11}+\nu_7=\nu_{12}+\nu_8=\nu_4$;
 $2\nu_{10}=\nu_{10}+\nu_8=\nu_{12}+\nu_8=\nu_5$; $2\nu_{10}=2\nu_{12}=\nu_{10}+\nu_8=\nu_{12}+\nu_8=\nu_{12}+\nu_{10}=\nu_6$; & $2\nu_{10}=2\nu_{11}=2\nu_{12}=\nu_{12}+\nu_{10}=\nu_7$.
 Accuracy of these methods compared to experimental benchmarks for F12-TcCR QFF
 VPT2 anharmonic vibrational frequencies are typically within 1.5% of their experimental
 values (Watrous et al. 2021).

2.2. Anharmonic Cascade Emission Spectrum

The simulation of an anharmonic cascade emission spectrum has been described previously in detail by Basire et al. (2011) and Mackie et al. (2018b). In this present study, a new, composite scheme is used to produce the emission spectrum of *cis-cis* and *cis-trans* carbonic acid. This composite scheme involves the use anharmonicity constants (χ) and vibrational frequencies from the F12-TcCR method and IR intensities from 2^{nd} order Møller-Plesset perturbation theory, MP2 (Møller & Plesset 1934), which has been shown to provide notable accuracy for less cost compared to higher-level methods for intensities (Finney et al. 2016). The F12-TcCR frequencies are obtained from the above-described QFF procedure. The MP2 portion begins with computation of the optimized geometry followed by computation of the harmonic normal modes and, finally, that of the quadratic, cubic, and quartic normal coordinate force constants giving the MP2/aug-cc-pVTZ QFF of *cis-cis* and *cis-trans* carbonic acid utilizing Gaussian 16 (Frisch et al. 2016; Dunning 1989; Peterson & Dunning 1995; Kendall et al. 1992). To properly treat resonances, a locally modified version of SPECTRO (Gaw et al. 1991) is used to compute the anharmonic vibrational absorption spectrum. SPECTRO takes the optimized geometry and QFF as input. The QFF is computed in normal mode coordinates, and a linear transformation is performed to produce a Cartesian coordinate QFF. The resonances are determined via two parameters: the difference in energy between the two states (Δ) set to the default value of

200 cm^{-1} , and the minimum value of the interaction between the two states (W) is also set to the default value of 10 cm^{-1} . Resonance polyads have the added advantage of allowing for intensity redistribution among modes based on the contribution of each mode to the final perturbed mode frequency resulting from the resonance analysis to calculate the IR intensities more accurately. This procedure produces the MP2/aug-cc-pVTZ anharmonic IR intensities utilized in the cascade emission simulations.

A vibrationally excited molecule in a collision-free environment radiatively relaxes by emitting IR photons until all of the energy is dissipated. The probability of emitting an IR photon at a given internal energy is proportional to the magnitude of the vibrational frequency of the corresponding normal mode multiplied by the energy-dependent emission at the given internal energy. This process is modeled via a straightforward cascade emission process (Cook & Saykally 1998; Pech et al. 2002; Basire et al. 2011; Mackie et al. 2018a). In short, a Wang-Landau walk is used to calculate the density of states followed by a second Wang-Landau random walk to produce an energy-dependent spectrum. From there, an IR photon is chosen based on the criteria described above resulting in the energy loss of the IR photon. At this new internal energy, the energy-dependent emission spectrum is recalculated, giving a new set of emission probabilities. This is repeated until the molecule has relaxed to its vibrational ground state, and the entire process is repeated until the desired accuracy is achieved yielding a cascade emission spectrum. Each simulation is run with varying internal excitation energies of 1 eV, 2 eV, 3 eV, and 4 eV using 2×10^6 photons.

3. Results

Table 1 immediately shows the quality of the F12-TcCR QFF results for the known rotational constants. Differences in the principle rotational constants between quantum

Table 1: The F12-TcCR, and Experimental Rotational Constants for *cis-cis*- and *cis-trans*-Carbonic Acid.

Constant	Units	<i>cis-cis</i>		<i>cis-trans</i>	
		F12-TcCR	Exp. ^a	F12-TcCR	Exp. ^b
A_e	MHz	12071.1		11877.8	
B_e	MHz	11397.2		11493.4	
C_e	MHz	5862.1		5841.2	
A_0	MHz	11998.8	11997.0550	11780.4	11778.6808
B_0	MHz	11311.5	11308.3803	11426.4	11423.1345
C_0	MHz	5814.9	5813.828	5793.2	5792.0741
Δ_J	kHz	6.259	6.165	5.451	5.73
Δ_K	kHz	9.475	6.0	6.933	8.14
Δ_{JK}	kHz	-3.533	-1.5	0.578	-1.16
δ_J	kHz	2.698	2.618	2.286	2.618
δ_K	kHz	5.153	6.28	5.643	6.28
Φ_J	mHz	7.893		3.156	
Φ_K	mHz	181.354		153.699	
Φ_{JK}	mHz	47.549		66.346	
Φ_{KJ}	mHz	-204.683		-195.106	
ϕ_j	mHz	3.966		1.605	
ϕ_{jk}	mHz	28.260		33.132	
ϕ_k	mHz	17.301		20.206	

^aMori et al. (2011).

^bMori et al. (2009).

chemical computations and experiment are roughly 3 MHz or less or errors of less than 0.03%. Hence, this quantum chemical approach is producing exceptional accuracy boding well for other spectroscopic properties. This accuracy continues in large part for the quartic distortion constants in Table 1, and the sextic distortion constants are provided in this work for the first time for high-precision comparison. However, the IR, vibrational features are much more novel and pressing for potential JWST observations.

Table 2: The F12-TcCR, Previous, and Experimental Fundamental Vibrational Frequencies for *cis-cis*-Carbonic Acid in cm^{-1} with Intensities (f) in km/mol .^a

	Description	F12-TcCR	MP2		ωB97XD^a	Exp. ^b
			Freqs.	f		
$\omega_1 (a_1)$	O–H symm. stretch	3826.2	3825.6	15	3833	
$\omega_2 (b_2)$	O–H antisymm. stretch	3823.6	3825.2	208	3880	
$\omega_3 (a_1)$	C=O stretch	1846.1	1847.9	521	1860	
$\omega_4 (b_2)$	C–O antisymm. stretch	1487.6	1474.0	144	1488	
$\omega_5 (a_1)$	C–O–H symm. bend	1308.6	1297.4	31	1298	
$\omega_6 (b_2)$	C–O–H antisymm. bend	1182.2	1171.0	437	1177	
$\omega_7 (a_1)$	C–O symm. stretch	989.2	992.5	20	1005	
$\omega_8 (b_1)$	CO ₃ OPB	808.5	814.3	40	822	
$\omega_9 (b_2)$	O–C–O antisymm. bend	607.8	606.2	211	604	
$\omega_{10} (b_1)$	C–O–H symm. OPB	603.0	619.2	47	612	
$\omega_{11} (a_1)$	O–C–O symm. bend	552.4	556.5	6	556	
$\omega_{12} (a_2)$	H–O–C symm. OPB	531.7	533.3	–	539	
$\nu_1 (a_1)$	O–H symm. stretch	3637.7	3639.5	13	3641	3634
$\nu_2 (b_2)$	O–H antisymm. stretch	3634.9	3639.3	190	3638	3630
$\nu_3 (a_1)$	C=O stretch	1804.9	1812.6	401	1829	1783
$\nu_4 (b_2)$	C–O antisymm. stretch	1438.5	1434.3	118	1452	1456
$\nu_5 (a_1)$	C–O–H symm. bend	1261.2	1252.6	31	1234	
$\nu_6 (b_2)$	C–O–H antisymm. bend	1143.7	1130.6	403	1117	1187
$\nu_7 (a_1)$	C–O symm. stretch	963.0	968.1	15	987	
$\nu_8 (b_1)$	CO ₃ OPB	793.5	799.0	36	802	798
$\nu_9 (b_1)$	O–C–O antisymm. bend	603.4	601.2	207	396	
$\nu_{10} (a_1)$	C–O–H symm. OPB	571.2	573.5	44	610	
$\nu_{11} (b_2)$	O–C–O symm. bend	546.8	548.8	6	547	
$\nu_{12} (a_2)$	H–O–C symm. OPB	509.8	512.5	–	309	
ZPVE		8664.6				
$2\nu_7$		1932.9	1933.4	10		
$\nu_{11} + \nu_5$		1820.1	1798.1	84		
$\nu_{12} + \nu_8$		1340.1	1307.4	45		
$\nu_{11} + \nu_9$		1151.4	1150.9	11		

^aHuber et al. (2012).

^bNe matrix data from Bernard et al. (2011).

3.1. *cis-cis*-Carbonic Acid Fundamental Vibrational Frequencies

The F12-TcCR anharmonic frequencies and MP2 anharmonic intensities, however, showcase that not only does carbonic acid have large IR intensities, but *cis-cis*-carbonic acid has larger intensities than the *cis-trans*. Hence, the lower-energy conformer should be more observable in the IR than the radioastronomically-observed form. Table 2 shows the vibrational spectral data for *cis-cis*-carbonic acid. The ν_3 C=O, ketone stretch and the ν_6 C–O–H antisymmetric bend exhibit the largest intensities at roughly 400 km mol^{-1} . For reference, the “bright” antisymmetric stretch in water is a factor of more than five lower at roughly 70 km mol^{-1} . As such, the perceived accuracy of the F12-TcCR QFF implies that absorption features at 1804.9 cm^{-1} ($5.54 \mu\text{m}$) and 1143.7 cm^{-1} ($8.74 \mu\text{m}$), respectively for ν_3 and ν_6 , should be markers of possible carbonic acid.

The *cis-cis*-carbonic acid conformer also has large intensities for many other fundamental vibrational frequencies, including in the hydride stretching region, especially for ν_2 at 3634.9 cm^{-1} ($2.75 \mu\text{m}$). Unfortunately, this fundamental lies roughly 20 cm^{-1} lower in frequency than the less intense symmetric stretch of water at $2.73 \mu\text{m}$. Hence, distinction between water and carbonic acid here would be challenging. At the other end of the frequency regime, the ν_9 in-plane bending of the ketone oxygen (the O–C–O antisymmetric bend) also exhibits a large intensity of roughly 200 km mol^{-1} . This 603.4 cm^{-1} ($16.57 \mu\text{m}$) absorption bookends the strong features for this conformer. Other notable IR absorptions include ν_4 as well as the $\nu_{11} + \nu_5$ combination band.

Additionally, the correlation between the F12-TcCR QFF fundamental anharmonic vibrational frequencies and those from Ne matrix data (Bernard et al. 2011) are largely in line with what is accepted as differences brought about by matrix shifts. The biggest question mark comes from ν_6 where the Ne matrix frequency of 1187 cm^{-1} is higher than all reported, computed frequencies. This could be a misassignment, but the large intensity

of the fundamental transition should make this frequency stand out, casting doubt on any improperly attributed peaks. Hence, the relatively large matrix shift is likely real and may result from the fundamentals changing frequency such that the $\nu_{12} + \nu_8 = \nu_{12} + \nu_{10} = \nu_6$ Fermi resonance polyad is broken. In any case, the correlation between levels of theory for F12-TcCR and MP2 is also exceptional with all fundamentals in alignment of better than 8.0 cm^{-1} save for, again, ν_6 at 13.1 cm^{-1} . Regardless, the QFF appears to be performing well, implying that the rotational constants are reliable and that the present results will be valuable in the determination of IR spectral features for this lowest energy form of carbonic acid.

3.2. *cis-trans*-Carbonic Acid Fundamental Vibrational Frequencies

The story for *cis-trans*-carbonic acid mirrors the *cis-cis* quite closely as shown in Table 3. The biggest difference comes in the intensities of the fundamentals. None are above 250 km/mol , but ν_3 , ν_4 , ν_6 , and ν_{12} are all in the roughly 200 km mol^{-1} to 250 km mol^{-1} range. The ν_3 ketone stretch is, once more, a major contributor to the overall intensity budget for this IR spectrum. This *cis-trans*-carbonic acid C=O stretch is black-shifted to 1847.4 cm^{-1} ($5.41 \mu\text{m}$) compared to the other conformer, but these distinct differences are still not too far away from one another such that this could make for a nice pairing that would aid in gas-phase observation of both conformers at once. The $\nu_9 + \nu_5$ combination band at 1867.7 cm^{-1} ($5.35 \mu\text{m}$) will also add features to the $5 \mu\text{m}$ region with its intensity of 162 km mol^{-1} , again more than twice the standard candle in the antisymmetric stretch of water.

The breaking of the symmetry from C_{2v} in the *cis-cis* to C_s here in the *cis-trans* decouples modes that would contribute to larger intensities, but similar motions are producing the largest intensity transitions. For instance, the ν_4 and ν_5 C–O–H bends have similar intensities but are split 140 cm^{-1} apart. Differently, the ν_{12} OPB motion is the only

Table 3: The F12-TcCR, Previous, and Experimental Fundamental Vibrational Frequencies for *cis-trans*-Carbonic Acid in cm^{-1} with Intensities (f) in km/mol .^a

	Description	F12-TcCR	MP2		ωB97XD^a	Exp. ^b
			Freqs.	f		
$\omega_1 (a')$	O–H ₂ stretch	3825.1	3805.0	108		
$\omega_2 (a')$	O–H ₁ stretch	3820.1	3797.4	101		
$\omega_3 (a')$	C=O stretch	1897.1	1880.6	474		
$\omega_4 (a')$	C–O–H ₁ bend	1430.9	1408.9	305		
$\omega_5 (a')$	C–O–H ₂ bend	1289.1	1270.2	119		
$\omega_6 (a')$	C–O ₂ stretch	1175.8	1159.4	201		
$\omega_7 (a')$	C–O ₁ stretch	977.2	967.9	46		
$\omega_8 (a'')$	CO ₃ OPB	795.1	790.2	24		
$\omega_9 (a')$	O–C–O ₂ bend	613.4	605.8	9		
$\omega_{10} (a'')$	C–O–H ₁ OPB	569.3	571.7	13		
$\omega_{11} (a')$	O–C–O ₁ bend	549.7	544.6	27		
$\omega_{12} (a'')$	C–O–H ₂ OPB	491.3	495.7	211		
$\nu_1 (a')$	O–H ₂ stretch	3637.7	3625.1	98	3770	3628
$\nu_2 (a')$	O–H ₁ stretch	3632.5	3615.4	88	3739	
$\nu_3 (a')$	C=O stretch	1847.4	1845.1	242	1873	1836
$\nu_4 (a')$	C–O–H ₁ bend	1385.7	1370.1	236	1386	1427
$\nu_5 (a')$	C–O–H ₂ bend	1253.5	1220.8	176	1253	
$\nu_6 (a')$	C–O ₂ stretch	1134.6	1123.1	201	1123	1184
$\nu_7 (a')$	C–O ₁ stretch	948.1	943.1	45	969	
$\nu_8 (a')$	CO ₃ OPB	785.7	778.5	21	798	784
$\nu_9 (a')$	O–C–O ₂ bend	608.2	600.7	8	614	
$\nu_{10} (a'')$	C–O–H ₁ OPB	545.8	540.8	24	632	
$\nu_{11} (a'')$	O–C–O ₁ bend	544.8	539.0	26	540	
$\nu_{12} (a'')$	C–O–H ₂ OPB	477.2	474.4	195	529	
ZPVE		8601.8				
$2\nu_7$		1911.4	1885.7	46		
$\nu_9 + \nu_5$		1867.7	1829.7	162		
$\nu_{10} + \nu_8$		1336.3	1327.9	64		
$\nu_{11} + \nu_{10}$		1091.0	1140.0	12		
$\nu_{12} + \nu_{11}$		1022.8	1256.7	13		

^aHuber et al. (2012).

^bNe matrix data from Bernard et al. (2011).

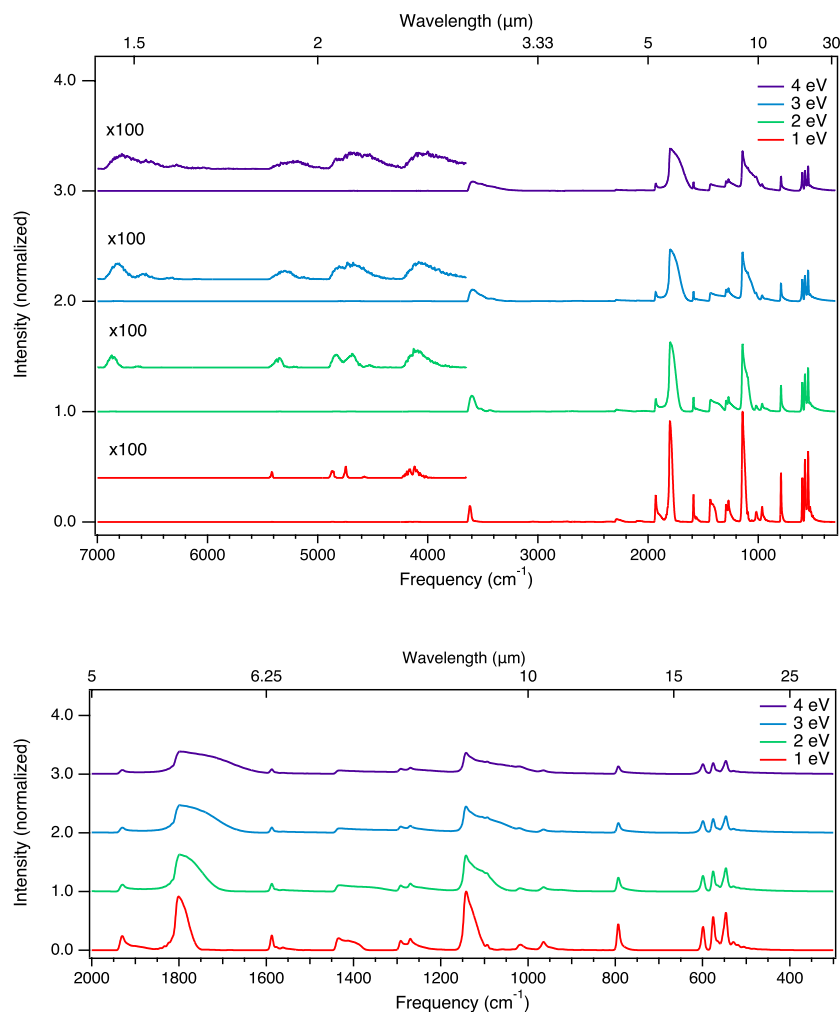
one of its kind to showcase a large intensity. This fundamental at 477.2 cm^{-1} ($20.96\text{ }\mu\text{m}$) is also the lowest-frequency for either form of carbonic acid.

Correlation between F12-TcCR and MP2 QFFs is similar in this conformer as it is in *cis-cis*-carbonic acid. Comparison to Ne matrix data still exhibits a large matrix shift for ν_6 , but this conformer also has a large matrix shift in ν_4 , as well. These matrix shifts are all to lower-frequency gas-phase fundamentals implying that either the polyads shift or the matrix is behaving in non-standard ways; further gas-phase experimental characterization for IR fundamental frequencies would help to settle these discrepancies. Regardless, the computed and experimental frequencies are within a few dozen cm^{-1} of one another, and the QFF is not exhibiting any questionable behaviors. As such, the presently-computed frequencies should be reliable proxies for gas-phase results potentially more so than the matrix data. The theoretical results are also complete and step beyond the density functional theory computations utilized to assign the matrix spectral features (Bernard et al. 2011).

3.3. Cascade Emission Spectra

The full emission spectrum of *cis-cis*-carbonic acid is given in the top of Figure 1 showcasing how the above-discussed F12-TcCR anharmonic fundamental vibrational features will emit when excited to the given internal energy. The tallest emission features line up with the initial energy levels discussed above (and given in Table 2), but the full cascade computed herein gives shape to the emissions. Of course, the most notable features correspond to ν_3 and ν_6 , and as more energy is added to the initial excitation, the red wings of the emission are broader as shown previously (Mackie et al. 2022). They even begin to mix and combine beyond 2 eV. Additionally, the low-frequency range from 600 cm^{-1} and below ($16.67\text{ }\mu\text{m}$ and longer) shows intensity borrowing from ν_9 given to ν_{10} and ν_{11} such that the least intense absorption in ν_{11} (6 km mol^{-1}) actually has the most intense emission

Fig. 1.— Total (top) and 2000 - 300 cm^{-1} range (bottom) anharmonic cascade emission spectra of *cis-cis*-carbonic acid at excitation energies of 1, 2, 3, and 4 eV calculated with the F12-TcCR & MP2/aug-cc-pVTZ composite scheme. The intensity of the spectra from 7000 - 3600 cm^{-1} are expanded by a factor of 100 to show the detail of the minor features.

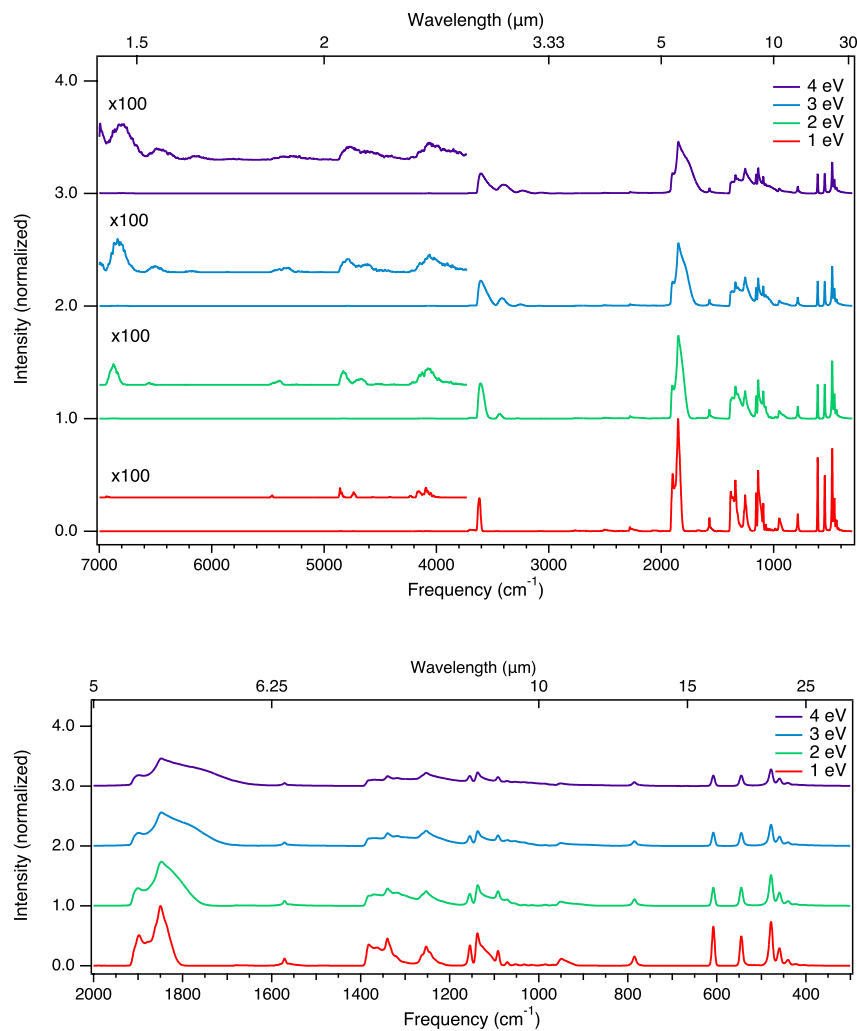


for this triplet of emission peaks shown in more detail in the bottom of Figure 1.

Figure 2 showcases the same data for the *cis-trans* conformer. While similar in many ways, the slight shifts of the fundamentals between molecular structures are born out in the emissions. Here, the leading, tall peak at $\sim 1900\text{ cm}^{-1}$ ($\sim 5.5\text{ }\mu\text{m}$) is mixed with the preceding and trailing ones since $2\nu_7$, $\nu_9 + \nu_6$, and the fundamental ν_3 are all emitting within the same region. As a consequence of this and also as the internal energy increases, the width of the red wing increases notably due to the presence of all three of these modes where the bottom of Figure 2 highlights this more clearly. Additionally, the hydride stretching region at 3600 cm^{-1} exhibits more structure in this less stable conformer than the *cis-cis*. While a quick visual inspection could lead one to think that Figures 1 and 2 are qualitatively similar, they have some differences on the more quantitative scale that will show distinct vibrational structure upon observation.

These emission spectra allow for direct comparison to JWST (or archival, predecessor mission) observations as well as laboratory simulations for interstellar spectral data. The most obvious difference between these carbonic acid emissions and those from IR observations is that the hydride stretches are at shorter wavelengths due to the nature of O–H stretching as opposed to C–H stretching at $\sim 3.3\text{ }\mu\text{m}$ believed to originate with polycyclic aromatic hydrocarbons (PAHs) (Allamandola et al. 1999; Peeters et al. 2004; Tielens 2008; Boersma et al. 2011; Allamandola et al. 2021). Hence, while the hydride stretches in carbonic acid are not the most intense or the brightest emitters for these molecules, they may be among the best ones to observe due to a combination of the higher resolution of JWST’s NIRSpec instrument and the lack of crowding by most PAH features. Water will, again, affect this region of the spectrum, but the resolution of JWST may allow for these to be distinguished. Unfortunately, for either isomer of carbonic acid, interstellar IR emissions from $5.5\text{ }\mu\text{m}$ to $6.0\text{ }\mu\text{m}$ are populated with what are believed to be some PAH

Fig. 2.— Total (top) and 2000 - 300 cm^{-1} range (bottom) anharmonic cascade emission spectra of *cis-trans*-carbonic acid at excitation energies of 1, 2, 3, and 4 eV calculated with the F12-TcCR & MP2/aug-cc-pVTZ composite scheme. The intensity of the spectra from 7000 - 3600 cm^{-1} are expanded by a factor of 100 to show the detail of the minor features.



features, but these $\sim 5.5 \mu\text{m}$ features are not as numerous or strong as those at $3.3 \mu\text{m}$, $6.2 \mu\text{m}$, $7.7 \mu\text{m}$, $8.6 \mu\text{m}$, etc. Hence, carbonic acid may yet be observable with JWST's MIRI instrument in this range for both conformers' strongest emission features. The sub 1400 cm^{-1} ($7.1 \mu\text{m}$ and longer) features of either carbonic acid isomer will likely be completely covered by PAH features but could play a role in these regions, as well.

4. Conclusions

The IR wavelengths around $2.75 \mu\text{m}$ or between $5.5 \mu\text{m}$ and $6.0 \mu\text{m}$ would likely be the best region to observe emission from carbonic acid in either conformer. The lower-energy, as-of-yet unobserved *cis-cis* conformer has larger IR intensities than the observed, less stable *cis-trans* conformer implying that either JWST NIRSpec or MIRI observations could indicate the presence of *cis-cis*- H_2CO_3 , whereas radioastronomical observations likely cannot. While both molecules exhibit similar features qualitatively, they have little direct overlap quantitatively. Most fundamental vibrational transitions differ between the molecules by 50 cm^{-1} or so making spectral deviations between conformers readily discernible with JWST. While most of the features for carbonic acid are in regions dominated by PAHs, the higher-frequency, shorter-wavelengths, again, are the best bet for observing this molecule in the IR provided that water features do not cause different opacity issues for carbonic acid.

The presence of *cis-cis*-carbonic acid is almost a given with the known observation of the *cis-trans* conformer. The barrier to rotation is fairly low, and similar chemical processes should produce both conformers. While the formation of carbonic acid from *trans*-HOCO and hydroxyl radicals on a grain surface would lead preferentially to the *cis-trans*-carbonic acid conformer, numerous other reactions can produce this molecule which tautomerizes to astrochemically abundant carbon dioxide and water. Carbonic acid in any form stands to

greatly enhance astrobiological insights and expand the census of relatively simple organic molecules in space. Its possession of a ketone as well as two alcohols makes it a useful intermediate between carbon dioxide/water and prebiotic species, and this molecule is likely present in astronomical environments stretching from disks to planetary atmospheres to, obviously, molecular clouds in the ISM. Now that the full IR spectrum in absorption and emission has been produced herein, further exploration for its presence in space can be undertaken.

5. Acknowledgements

RCF acknowledges support from NASA grants NNX17AH15G & NNH22ZHA004C, NSF grant OIA-1757220, and start-up funds provided by the University of Mississippi. VJE acknowledges support from the NASA Postdoctoral Program. Both authors, RCF and VJE, acknowledge support from the Internal Scientist Funding Model (ISFM) Laboratory Astrophysics Directed Work Package at NASA Ames (22-A22ISFM-0009). Additionally, the authors would like to thank Izaskun M. Jiménez-Serra of El Centro de Astrobiología (CAB), INTA-CSIC in Spain for inspiration for and discussions of this research project as well as Alexandros Maragkoudakis of the NASA Ames Research Center for ideas about how these data could influence JWST observations.

REFERENCES

- Adler, T. B., Knizia, G., & Werner, H.-J. 2007, *J. Chem. Phys.*, 127, 221106
- Allamandola, L. J., Boersma, C., Lee, T. J., Bregman, J. D., & Temi, P. 2021, *Astrophys. J.*, 917, L35
- Allamandola, L. J., Hudgins, D. M., & Sandford, S. A. 1999, *Astrophys. J.*, 511, L115
- Basire, M., Parneix, P., Pino, T., Bréchnignac, P., & Calvo, F. 2011, in *PAHs and the Universe*, ed. C. Joblin & A. Tielens, Vol. 46 (EAS Publications Series), 95–101
- Bernard, J., Seidl, M., Kohl, I., et al. 2011, *Angew. Chem. Int. Ed.*, 50, 1939
- Boersma, C., Bauschlicher, Jr., C. W., Ricca, A., et al. 2011, *Astrophys. J.*, 729, 64
- Cook, D. J., & Saykally, R. J. 1998, *Astrophys. J.*, 493, 793
- Crawford, T. D., & Schaefer III, H. F. 2000, in *Reviews in Computational Chemistry*, ed. K. B. Lipkowitz & D. B. Boyd, Vol. 14 (New York: Wiley), 33–136
- Davis, M. C., Garrett, N. R., & Fortenberry, R. C. 2022, *Phys. Chem. Chem. Phys.*, 24, 18552
- Douglas, M., & Kroll, N. M. 1974, *Ann. Phys.*, 82, 89
- Dunning, T. H. 1989, *J. Chem. Phys.*, 90, 1007
- Finney, B., Fortenberry, R. C., Francisco, J. S., & Peterson, K. A. 2016, *J. Chem. Phys.*, 145, 124311
- Fortenberry, R. C., & Lee, T. J. 2019, *Ann. Rep. Comput. Chem.*, 15, 173
- . 2022, in *Vibrational Dynamics of Molecules*, ed. J. M. Bowman (Singapore: World Scientific), 235–295

- Frisch, M. J., Trucks, G. W., Schlegel, H. B., et al. 2016, Gaussian 16 Revision C.01, gaussian Inc. Wallingford CT
- Gaw, J. F., Willets, A., Green, W. H., & Handy, N. C. 1991, in *Advances in Molecular Vibrations and Collision Dynamics*, ed. J. M. Bowman & M. A. Ratner (Greenwich, Connecticut: JAI Press, Inc.), 170–185
- Györfy, W., & Werner, H.-J. 2018, *J. Chem. Phys.*, 148, 114104
- Haney, O. G., Westbrook, B. R., Santaloci, T. J., & Fortenberry, R. C. 2023, *J. Phys. Chem. A*, 127, 489
- Hill, J. G., & Peterson, K. A. 2010, *Phys. Chem. Chem. Phys.*, 12, 10460
- Huber, S. E., Dalnobar, S., Kausch, W., Kimeswenger, S., & Probst, M. 2012, *AIP Adv.*, 2, 032180
- Ioppolo, S., Kanuchová, Z., James, R. L., et al. 2021, *Astron. Astrophys.*, 646, A172
- Jian, H.-Y., Yang, C.-T., & Chu, L.-K. 2021, *Phys. Chem. Chem. Phys.*, 23, 14699
- Jones, B. M., Kaiser, R. I., & Strazzulla, G. 2014, *Astrophys. J.*, 788, 170
- Kendall, R. A., Dunning, T. H., & Harrison, R. J. 1992, *J. Chem. Phys.*, 96, 6796
- Knizia, G., Adler, T. B., & Werner, H.-J. 2009, *J. Chem. Phys.*, 130, 054104
- Kumar, P. P., Kalinichev, A. G., & Kirkpatrick, R. J. 2007, *J. Chem. Phys.*, 126, 204315
- Mackie, C. J., Candian, A., Lee, T. J., & Tielens, A. G. G. M. 2022, *J. Phys. Chem. A*, 126, 3198
- Mackie, C. J., Chen, T., Candian, A., Lee, T. J., & Tielens, A. G. G. M. 2018a, *J. Chem. Phys.*, 149, 134302

- Mackie, C. J., Candian, A., Huang, X., et al. 2018b, *Phys. Chem. Chem. Phys.*, 20, 1189
- Martin, J. M. L., Lee, T. J., & Taylor, P. R. 1998, *J. Chem. Phys.*, 108, 676
- Mills, I. M. 1972, in *Molecular Spectroscopy - Modern Research*, ed. K. N. Rao & C. W. Mathews (New York: Academic Press), 115–140
- Møller, C., & Plesset, M. S. 1934, *Phys. Rev.*, 46, 618
- Mori, T., Suma, K., Sumiyoshi, Y., & Endo, Y. 2009, *J. Chem. Phys.*, 130, 204308
- . 2011, *J. Chem. Phys.*, 134, 044319
- Noble, J. A., Dulieu, F., Congiu, E., & Fraser, H. J. 2011, *Astrophys. J.*, 735, 121
- Papousek, D., & Aliev, M. R. 1982, *Molecular Vibration-Rotation Spectra* (Amsterdam: Elsevier)
- Pech, C., Joblin, C., & Boissel, P. 2002, *Astron. Astrophys.*, 388, 639
- Peeters, E., Allamandola, L. J., Hudgins, D. M., Hony, S., & Tielens, A. G. G. M. 2004, in *Astrophysics of Dust*, ASP Conference Series, ed. A. N. Witt, G. C. Clayton, & B. T. Draine, Vol. 309 (San Francisco, CA: Astronomical Society of the Pacific), 141–162
- Peeters, Z., Hudson, R., Moore, M., & Lewis, A. 2010, *Icarus*, 210, 480
- Peterson, K. A., Adler, T. B., & Werner, H.-J. 2008, *J. Chem. Phys.*, 128, 084102
- Peterson, K. A., & Dunning, T. H. 1995, *J. Chem. Phys.*, 102, 2032
- . 2002, *J. Chem. Phys.*, 117, 10548
- Raghavachari, K., Trucks, G. W., Pople, J. A., & Head-Gordon, M. 1989, *Chem. Phys. Lett.*, 157, 479

- Reddy, S. K., Kulkarni, C. H., & Balasubramanian, S. 2012, *J. Phys. Chem. A*, 116, 1638
- Sagiv, L., Hirshberg, B., & Gerber, R. B. 2018, *Chem. Phys.*, 514, 44
- Sandford, S. A., Nuevo, M., Bera, P. P., & Lee, T. J. 2020, *Chem. Rev.*, 120, 4616
- Sanz-Novo, M., Rivilla, V. M., Jiménez-Serra, I., et al. 2023, *Astrophys. J.*, *accepted*
- Shavitt, I., & Bartlett, R. J. 2009, *Many-Body Methods in Chemistry and Physics: MBPT and Coupled-Cluster Theory* (Cambridge: Cambridge University Press)
- Strazzulla, G., Brucato, J. R., & Palumbo, M. E. 1996, *Plan. Space Sci.*, 44, 1447
- Tielens, A. G. G. M. 2008, *Annu. Rev. Astron. Astrophys.*, 46, 289
- Wallace, A. M., & Fortenberry, R. C. 2021, *J. Phys. Chem. A*, 125, 4589
- . 2022, *J. Phys. Chem. A*, 126, 3739
- Wang, X., & Bürgi, T. 2021, *Angew. Chem. Int. Ed.*, 60, 7860
- Watrous, A. G., Westbrook, B. R., & Fortenberry, R. C. 2021, *J. Phys. Chem. A*, 125, 10532
- Watson, J. K. G. 1977, in *Vibrational Spectra and Structure*, ed. J. R. Dearing (Amsterdam: Elsevier), 1–89
- Werner, H.-J., Knowles, P. J., Knizia, G., Manby, F. R., & Schütz, M. 2012, *WIREs Comput. Mol. Sci.*, 2, 242
- Werner, H.-J., Knowles, P. J., Knizia, G., et al. 2022, see <http://www.molpro.net>
- Westbrook, B. R., & Fortenberry, R. C. 2020, *J. Phys. Chem. A*, 124, 3191
- . 2023, *J. Chem. Theory Comput.*, 19, 2606
- Yousaf, K. E., & Peterson, K. A. 2008, *J. Chem. Phys.*, 129, 184108

Zheng, W., & Kaiser, R. I. 2007, Chem. Phys. Lett., 450, 55

Zhu, C., Hosokai, S., & Akiyama, T. 2011, Crys. Growth Des., 11, 4166

This manuscript was prepared with the AAS L^AT_EX macros v5.2.